Grain boundary disordering in binary alloys

Jian Luo[a] and Xiaomeng Shi
School of Materials Science and Engineering, Clemson University, Clemson, South Carolina 29634, USA

(Received 29 January 2008; accepted 12 February 2008; published online 10 March 2008)

This letter reports a grain boundary (GB) premelting/prewetting model based on the Miedema model and computational thermodynamics, predicting that GB disordering can start at as low as 60%–85% of the bulk solidus temperatures in selected systems. This model quantitatively explains the long-standing mystery of subsolidus activated sintering in W–Pd, W–Ni, W–Co, W–Fe and W–Cu, and it has broad applications for understanding GB-controlled transport kinetics and physical properties. Furthermore, this study demonstrates the necessity of developing GB "phase" diagrams as a tool for material design. © *2008 American Institute of Physics*.
[DOI: 10.1063/1.2892631]

While the importance of surface premelting has been well recognized,[1] grain boundary (GB) premelting in unary systems was believed to be generally unimportant for material fabrication since Hsieh and Balluffi found that it does not occur up to a temperature of $0.999T_{\text{melt}}$ for pure Al.[2] On the other hand, stabilization of impurity-based, quasiliquid intergranular films (IGFs) at subsolidus temperatures has been observed in several binary and multicomponent materials, where an analogy to premelting in unary systems was made.[3] Tang *et al.*[4] proposed to understand subsolidus IGFs in binary systems from coupled GB premelting[1] and prewetting[5] transitions, where, in principle, concurrent GB adsorption can stabilize disordered IGFs over larger undercooling ranges.

In a classic review article[6] in 1978, Coble and Cannon stated that "the most significant changes which have been taken place in recent years regard the finding with respect to densification below the eutectics in numerous systems, notably tungsten-carbide:cobalt, tungsten:nickel,…" The exact underlying mechanism remained controversial for decades. Recent high-resolution transmission electron microscopy (HRTEM) studies attributed subsolidus activated sintering in Ni-doped W,[7,8] Bi_2O_3-doped ZnO,[9] and other systems[10] to short-circuit diffusion in premelting-like IGFs. Subsolidus activated sintering experiments have been conducted for W using various dopants with significantly different effectiveness,[11,12] enabling a critical test of the hypothesized sintering mechanism. Moreover, using onset sintering as an indicator for GB disordering, we can establish a quantitative model for predicting GB disordering in binary alloys with broader applications beyond sintering.

Five W alloys (W–M; M=Pd, Ni, Fe, Co, and Cu) are selected for this study in part due to the availability of binary thermodynamic functions [developed via the CALPHAD (CALculation of PHAse Diagrams) effort].[13,14] Stabilization of a subsolidus quasiliquid IGF of thickness h can be considered in terms of the free energy penalty for forming an undercooled liquid ($\Delta G_{\text{amorph}}h$) being more than offset by the reduction in interfacial energies resulting from the replacement of a GB with two crystal-liquid interfaces,

$$\Delta G_{\text{amorph}}h < (\gamma_{\text{GB}}^{(0)} - 2\gamma_{\text{cl}}) \equiv -\Delta\gamma. \tag{1}$$

The average excess free energy of random W GBs without adsorption ($\gamma_{\text{GB}}^{(0)}$) is interpolated from the data at 1773 K (1.08 J/m^2) (Ref. 15) and 0 K (1.225 J/m^2).[16] The crystal-liquid interfacial energies are estimated based on the Miedema model[16,17] and the data in Ref. 16,

$$\gamma_{\text{cl}} = F_M^{\text{W}}(X_M)\frac{\Delta H_{\text{W in }M}^{\text{interface}}}{C_0 V_{\text{W}}^{2/3}} + \frac{H_{\text{W}}^{\text{fuse}}}{C_0 V_{\text{W}}^{2/3}} + \frac{1.9RT}{C_0 V_{\text{W}M}^{2/3}}, \tag{2}$$

where $\Delta H_{\text{W in }M}^{\text{interface}}$ is the enthalpy of solution; X_M is the molar fraction of M in the liquid (IGF); C_0 is a constant ($\approx 4.5\times 10^8$); V is the molar volume; R is the gas constant; and $F_M^{\text{W}}(X_M)$ is the degree to which W atoms are surrounded by M atoms.[17]

The value of ΔG_{amorph} can be computed from the liquid formation free energy and the chemical potentials set by the equilibrium bulk phase(s) via standard CALPHAD methods:

$$\Delta G_{\text{amorph}} = G_{\text{liquid}}^{f} - [X_M\mu_M + (1-X_M)\mu_{\text{W}}]. \tag{3}$$

Relevant bulk thermodynamic terms are calculated using PANDAT software and the thermodynamic functions in Refs. 13 and 14.

We define the following variable to represent the thermodynamic tendency to stabilize a quasiliquid IGF:

$$\lambda \equiv \max_{(0<X_M<1)}\left\{\frac{-\Delta\gamma(X_M)}{\Delta G_{\text{amorph}}(X_M)}\right\}, \tag{4}$$

which scales the actual (equilibrium) film thickness.

Furthermore, the excess free energy of a quasiliquid IGF can be written as[3]

$$G^x - \gamma_{\text{GB}}^{(0)} = \Delta G_{\text{amorph}}h + \Delta\gamma f(h), \tag{5}$$

where $f(h)$ is an interfacial coefficient that ranges from 0 to 1 as h increases from 0 to ∞, and $\sigma_{\text{interfacial}}(h) \equiv \Delta\gamma[f(h)-1]$ is a short-range interfacial interaction.[3] The equilibrium thickness (h_{EQ}) is determined by minimizing Eq. (5). If a continuum approximation can be adopted,

$$f(h) \approx 1 - e^{-h/\xi} \tag{6}$$

and $h_{\text{EQ}} \approx \xi\ln(\lambda/\xi)$, where ξ is a coherent length of ~0.3 nm.[3,18] Then, we estimate the range of GB solidus temperature (T_{GBS}) via

[a]Author to whom correspondence should be addressed. Electronic mail: jianluo@clemson.edu and jluo@alum.mit.edu.

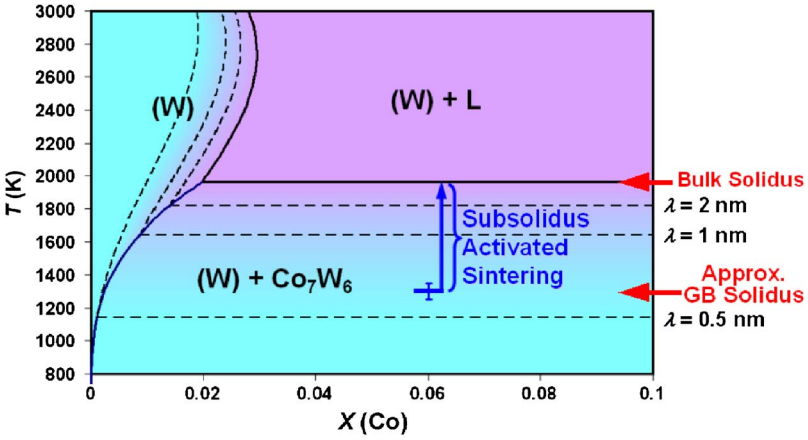

FIG. 1. (Color online) Computed lines of constant λ are plotted in the W–Co binary bulk phase diagram. Computed diagrams for W–Fe, W–Pd, and W–Ni exhibit similar features.

$$0.5\ \text{nm} < \lambda(T_{\text{GBS}}) < 1\ \text{nm}. \quad (7)$$

At T_{GBS}, h_{EQ} is about 1 monolayer (0.2–0.3 nm) from an extrapolation of the continuum approximation.

The λ values are computed numerically as functions of the bulk chemical potentials and temperature using a homemade MATLAB code. Lines of constant λ are plotted in bulk binary phase diagrams, and one example is shown in Fig. 1. At a constant temperature, λ is a constant in the two-phase region and decreases with decreasing dopant concentration in the single-phase region. Consistently, it is well known that additional doping beyond an optimal level (which is typically slightly above the solid solubility limits) does not provide additional benefits to enhance sintering.[7,11,12]

Subsequently, computed $\lambda(T)$ values for dopant-saturated W specimens (in the two-phase regions) are shown in Fig. 2, which predicts the correct order for the dopant effectiveness (Pd > Ni > Co ≈ Fe ≫ Cu).[11,12] Furthermore, $\lambda(T)$ can be used to rationalize detailed observations. For example, Pd is the most effective dopant at low temperatures, but Ni becomes more effective at moderate temperatures [inset in Fig. 2 (Ref. 11)]; this observation can be explained from the different slopes in $\lambda(T)$ (Fig. 2).

To conduct a critical model-experimental comparison, onset activated sintering temperatures are retrieved from prior studies[11,12] and normalized to remove variations due to the different sintering schemes and grain sizes. For GB-controlled sintering, it is known that $s^2 ds/dt \propto D_{\text{GB}} G^{-4}$, where s is the linear shrinkage, D_{GB} is the GB diffusivity, and G is the grain size. The onset activated sintering temperature is defined as the temperature at which $s^2 ds/dt = 10^{-8}\ \text{min}^{-1}$ for a reference grain size of 0.56 μm,[12] which corresponds to $s = 1\%$ after 33 min of isothermal sintering.

As shown in Table I, the normalized onset sintering temperatures fall into the estimated ranges of T_{GBS} for W–Pd, W–Ni, W–Co, and W–Fe, which are ~60%–85% of the bulk eutectic/peritectic temperatures ($T_{e/p}$). On the other hand, computed $\Delta\gamma$ is >0 for W–Cu, indicating that IGFs cannot form. This predication is consistent with the observation that Cu has no effect in enhancing sintering at all temperatures (Fig. 2),[11] even if this binary system has a low $T_{e/p}$ (Table I).

Recently, Tang *et al.* suggested an extension of the Gibbs definition of bulk phases to equilibrium GB features and designated them as *GB complexions*.[4,19] These subsolidus quasiliquid IGFs are one important GB complexion that is a precursor to the bulk liquid phase. Notably, Dillon and Harmer recently observed a series of GB complexions in doped Al_2O_3 with increasing levels of structural disorder and GB mobility, and their study explained the mechanism of abnormal grain growth (another outstanding scientific mystery).[19,20] To interpret their observations, Eq. (6) is refined to consider the finite atom size,

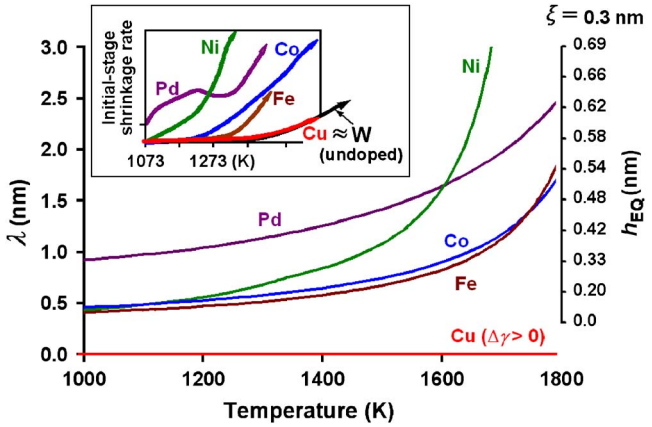

FIG. 2. (Color online) Computed λ vs T for dopant-saturated W specimens. Corresponding equilibrium film thicknesses are computed from a continuum approximation. The inset shows the T-dependent densification rates replotted after German and Munir (Fig. 5 in Ref. 11), where only initial-stage sintering data are included.

TABLE I. Onset activated sintering temperatures (T_{sinter}) vs estimated ranges of GB solidus temperatures (T_{GBS}). The $\Delta\gamma_{e/p}$ values are computed by using the eutectic/peritectic temperature ($T_{e/p}$) and composition. The listed T_{sinter} values are means (±standard deviations) of three sets of prior experimental data (Refs. 11 and 12). The first set of data are extrapolated from the isothermal sintering data (Refs. 11 and 12) and the other two sets are retrieved from continuous sintering experiments of 8.5 and 17 °C/min, where the original data (Ref. 11) have been numerically processed to obtain $s^2 ds/dt$.

	$T_{e/p}$ (K)	$\Delta\gamma_{e/p}$ (J/m^2)	T_{sinter} (K)	T_{GBS} (K)
W–Pd	2088	−0.60	1090 ± 23	<1141[a]
W–Ni	1768	−0.52	1150 ± 18	1121–1470
W-Co	1962	−0.40	1301 ± 49	1140–1644
W-Fe	1910	−0.37	1308 ± 50	1273–1664
W-Cu	1357	+0.49	No activated sintering	No IGF

[a]This estimation is less reliable than others because the thermodynamic functions for the W–Pd binary system have not been fully assessed [which were derived based on partial phase-diagram data (Ref. 14)].

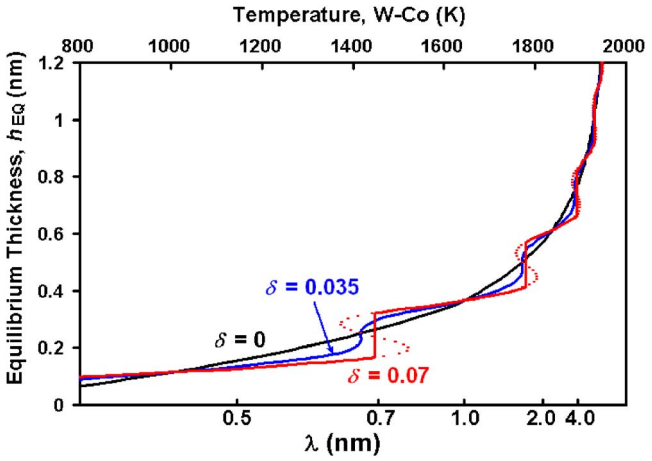

FIG. 3. (Color online) Computed equilibrium film thickness vs λ [using Eq. (8); ξ=0.3 nm]. Corresponding temperatures are computed for the W–Co system. Layering transitions occur for $\delta > 3.5\%$, leading to a series of GB complexions similar to those observed by Dillon and co-workers (Refs. 19 and 20).

$$f(h) \approx 1 - e^{-h/\xi}[1 - \delta \sin^2(\pi h/\sigma_0)], \tag{8}$$

where $\sigma_0 \approx 0.25$ nm is the interatomic distance. Equation (8) includes a well-known oscillatory structural force,[21] producing local energy minima at $h = n\sigma_0$ (n is an integer). This refinement leads to layering transitions[19,22] for moderate δ and produces to a series of GB complexions (Fig. 3) similar to those observed by Dillon and Harmer.[19,20]

The current model can be extended to multicomponent alloys via the use of well-established CALPHAD extrapolation methods and statistical thermodynamic models for estimating interfacial energies. This model for metals serves as a basis for developing models for ceramics, where London dispersion forces and electrostatic interactions should be added separately.[3] To accurately represent interfacial forces, additional coarse-grained parameters, e.g., the average film composition (X) and structural order (η), can be included in the interfacial coefficient $[f(h, X, \eta)]$ in Eqs. (5) and (6), which can, in principle, produce many different types of GB complexions and transitions. A further extension of this model should consider structural and chemical gradients in a diffuse-interface theory.[4]

In summary, a quantitative GB disordering model (with no adjustable parameters) can explain all major observations of subsolidus activated sintering. In conjunction with recent direct HRTEM observations,[7,8] it is concluded that subsolidus activated sintering is due to short-circuit diffusion in premelting-like IGFs. Moreover, this model can have broad applications beyond sintering, e.g., in understanding creep and liquid metal embrittlement.[3]

This study represents an initial step toward a long-range scientific goal of developing quantitative GB complexion (phase) diagrams as fundamental information leading to controlled material design. Because GB disordering or transitions can vastly change GB diffusivity and mobility, Fig. 1 and similar or more sophisticated diagrams (which may include first-order GB transitions[4]) can be used to design fabrication pathways to utilize desired GB structures during processing to control microstructural evolution. This study shows that bulk phase diagrams are not adequate for predicting optimal activated sintering protocols since liquidlike GB complexions can form at as low as 60%–85% of bulk solidus temperatures, resulting in subsolidus activated sintering (with phenomenological similarities to liquid-phase sintering). Furthermore, since IGFs or other GB complexions can be retained upon cooling and critically affect a variety of mechanical and physical properties,[3] GB complexion diagrams can also be used to devise heat treatment recipes to adjust final GB structures for the desired properties.

This research was supported by an AFOSR Young Investigator Award (No. FA9550-07-1-0125; High Temperature Aerospace Materials program, managed by Dr. Joan Fuller). We gratefully acknowledge the late Dr. R. M. Cannon for his deep insights. An open-source MATLAB code for computing Fig. 1 can be downloaded at http://alum.mit.edu/www/jluo/GB disorder/, and this annotated code can be adapted for modeling other binary alloys.

[1] J. G. Dash, A. M. Rempel, and J. S. Wettlaufer, Rev. Mod. Phys. **78**, 695 (2006).
[2] T. E. Hsieh and R. W. Balluffi, Acta Metall. **37**, 1637 (1989).
[3] J. Luo, Crit. Rev. Solid State Mater. Sci. **32**, 67 (2007).
[4] M. Tang, W. C. Carter, and R. M. Cannon, Phys. Rev. Lett. **97**, 075502 (2006).
[5] J. W. Cahn, J. Chem. Phys. **66**, 3667 (1977).
[6] R. L. Coble and R. M. Cannon, in *Processing of Crystalline Ceramics*, edited by H. Palmour III, R. F. Davis, and T. M. Hare (Plenum, NY, 1978), pp. 151–170.
[7] V. K. Gupta, D. H. Yoon, H. M. Meyer III, and J. Luo, Acta Mater. **55**, 3131 (2007).
[8] J. Luo, V. K. Gupta, D. H. Yoon, and H. M. Meyer, Appl. Phys. Lett. **87**, 231902 (2005).
[9] J. Luo, H. Wang, and Y.-M. Chiang, J. Am. Ceram. Soc. **82**, 916 (1999).
[10] E. Jud, Z. Zhang, W. Sigle, and L. J. Gauckler, J. Electroceram. **16**, 191 (2006); Z. L. Zhang, S. A. Wilfried, M. Ruhle, E. Jud, and L. J. Gauckler, Acta Mater. **55**, 2907 (2007).
[11] R. M. German and Z. A. Munir, Metall. Trans. A **7A**, 1873 (1976).
[12] H. W. Hayden and J. H. Brophy, J. Electrochem. Soc. **110**, 805 (1963).
[13] A. F. Guillermet, Metall. Trans. A **20**, 935 (1989); P. Gustafson, Metall. Trans. A **18**, 175 (1987); P. Gustafson, Z. Metallkd. **79**, 388 (1988); P. Gustafson, A. Gabriel, and I. Ansara, Z. Metallkd. **78**, 151 (1987).
[14] S. K. Lee and D. N. Lee, CALPHAD: Comput. Coupling Phase Diagrams Thermochem. **10**, 61 (1986).
[15] E. N. Hodkin, M. G. Nicholas, and D. M. Poole, J. Less-Common Met. **20**, 93 (1970).
[16] F. R. de Boer, R. Boom, W. C. M. Mattens, A. R. Miedema, and A. K. Niessen, *Cohesion in Metals: Transition Metals Alloys* (North-Holland, Amsterdam, 1988).
[17] R. Benedictus, A. Böttger, and E. J. Mittemijer, Phys. Rev. B **54**, 9109 (1996).
[18] D. R. Clarke, J. Am. Ceram. Soc. **70**, 15 (1987).
[19] S. J. Dillon, M. Tang, W. C. Carter, and M. P. Harmer, Acta Mater. **55**, 6208 (2007).
[20] S. J. Dillon and M. P. Harmer, Acta Mater. **55**, 5247 (2007).
[21] J. N. Israelachvili, *Intermolecular and Surface Forces*, 4th ed. (Academic, London, 1994).
[22] R. Pandit, M. Schick, and M. Wortis, Phys. Rev. B **26**, 5112 (1982).